Improved nowcasting of precipitation based on convective analysis fields

T. Haiden and M. Steinheimer

Central Institute for Meteorology and Geodynamics (ZAMG), Vienna, Austria

Submitted to:

Advances in Geosciences

July 2006

Corresponding author: Thomas Haiden

Zentralanstalt für Meteorologie und Geodynamik

Hohe Warte 38, A-1190 Vienna, Austria

E-mail: thomas.haiden@zamg.ac.at

Abstract. The high-resolution analysis and nowcasting system INCA (**I**ntegrated **N**owcasting through **C**omprehensive **A**nalysis) developed at the Austrian national weather service provides three-dimensional fields of temperature, humidity, and wind on an hourly basis, and two-dimensional fields of precipitation rate in 15 minute intervals. The system operates on a horizontal resolution of 1 km and a vertical resolution of 100-200 m. It combines surface station data, remote sensing data (radar, satellite), forecast fields of the numerical weather prediction model ALADIN, and high-resolution topographic data.

An important application of the INCA system is nowcasting of convective precipitation. Based on fine-scale temperature, humidity, and wind analyses a number of convective analysis fields are routinely generated. These fields include convective boundary layer (CBL) flow convergence and specific humidity, lifted condensation level (LCL), convective available potential energy (CAPE), convective inhibition (CIN), and various convective stability indices. Based on the verification of areal precipitation nowcasts it is shown that the pure translational forecast of convective cells can be improved by using a decision algorithm which is based on a subset of the above fields, combined with visible satellite imagery.

1 Introduction

Most existing observation-based forecasting systems have been designed for the prediction of precipitation and convective phenomena (Browning and Collier 1989, Li et al. 1995, Hand 1996, Golding 1998, Pierce et al. 2000, Seed 2003). During the World Weather Research Program (WWRP) Forecast Demonstration Project (FDP) of the 2000 Sydney Olympics several systems were tested and compared (Pierce et al. 2004). A wind analysis and nowcasting system was also tested and evaluated during that project (Crook and Sun 2004). The work, however, was not primarily focused on the wind field as such but on its use for the prediction of the initiation and development of deep convection (Wilson and Schreiber 1986, Wilson et al. 2004). Similarly, analysis and nowcasting of near-surface temperature (Sun and Crook 2001) has been of interest mainly in the prediction of convective developments rather than as a forecast field in itself.

There is an increasing demand for automated high-quality very-short-range forecasts and nowcasts not just of precipitation but also temperature, wind, humidity, cloudiness, or global radiation. Real-time flood-warning systems based on detailed hydrological modeling require meteorological input on small scales and at high update frequencies. High-resolution road weather forecasts become increasingly important both for winter road management and for transportation planning. In response to these requirements the analysis and nowcasting system INCA (Integrated Nowcasting through Comprehensive Analysis) has been developed. Section 2 gives a short overview of its general characteristics, data sources, and the analysis and nowcasting methods used.

During the 2000 Sydney Olympics FDP several nowcasting systems were tested and evaluated (Pierce et al. 2004). They use different methods of determining precipitation movement such as area tracking, individual cell tracking, and NWP model winds. Two of the systems, namely GANDOLF (MetOffice, Exeter, UK) and ANC (NCAR, Boulder, CO, USA) also have convective evolution and initiation capability (Wilson et al. 2004). In the GANDOLF system, convective cells are classified into different stages of development. Based on a conceptual model of storm evolution, future states are predicted. New ('daughter') cells can be initiated close to existing cells if the boundary layer convergence predicted by the NWP model is sufficiently strong. The ANC predicts cell initiation and evolution based on the interaction of existing storms and cumulus clouds with boundary layer convergence lines observed by radar and predicted by NWP wind field characteristics. The main findings with regard to convective cell prediction in the Sydney FDP can be summarized as follows (Wilson et al., 2004): *1) Predictive skill above pure translation occurs when boundary layer convergence lines can be identified and used to nowcast cell evolution. 2) For nowcasts beyond 60 min, boundary characteristics are more important for storm initiation than early detection of cumulus clouds*.

For the development of a cell initiation and evolution module in INCA, described in Section 3, these results served as a guideline. They also indicate the importance of a good boundary-layer wind field analysis. In Austria's alpine terrain, boundary layer convergence lines are to a large degree related to topography, which adds a deterministic component to cell initiation (Haiden 2001). With the current version of the INCA wind field analysis, the ability to correctly detect these convergence lines critically depends on the skill of the ALADIN model in predicting them, and on the surface station network to represent them. Case studies are carried out to determine to what extent this is in fact the case. However, none of the systems used in the Sydney FDP used

convective analysis fields such as CAPE or CIN, so it is interesting to investigate what additional benefit can be gained from those. Results of the case studies are discussed in Section 4.

2 The INCA system

The basic structure of the INCA analysis and nowcasting system is shown in Figure 1. The forecast of a numerical weather prediction (NWP) model is trilinearly interpolated to the high-resolution (1 km) INCA grid, serving as a first guess. Differences between surface observations and the first guess are determined and spatially interpolated using inverse distance weighting (IDW) both in geometric and in physical space. In the case of temperature, for example, geometrical distance weighting is used in the horizontal, while in the vertical the distance weighting is performed in potential temperature space. The three-dimensional 'distance' between INCA gridpoint (*i*,*j*,*m*) and the *k*-th surface station is given by

$$r_{ijmk} = \sqrt{(x_k - x_i)^2 + (y_k - y_j)^2 + c^2(\theta_k^{NWP} - \theta_{ijm}^{NWP})^2}\,, \tag{1}$$

where the parameter *c* has the dimension of an inverse temperature gradient. The interpolated three-dimensional temperature difference field is obtained from

$$\Delta\theta(i,j,m) = \frac{\sum_k \dfrac{\theta_k^{OBS} - \theta_k^{NWP}}{r_{ijmk}^2}}{\sum_k \dfrac{1}{r_{ijmk}^2}} \tag{2}$$

and added to the NWP first guess, giving

$$\theta^{INCA}(i,j,m) = \theta^{NWP}(i,j,m) + \Delta\theta(i,j,m)\,. \tag{3}$$

Meteorological fields routinely analyzed with INCA are listed in Table 1. Analyses and nowcasts of these fields have been operational since 2005. The convective analysis fields are classical convective diagnostics such as lifted condensation level (LCL), convective available potential energy (CAPE), equivalent potential temperature, and various instability incices.

The high resolution of 1 km is an essential characteristic of INCA. It enables the system to process locally influenced station observations, because at this resolution the actual elevation and exposition of most surface stations coincides reasonably well with the corresponding values on the numerical grid. In steep terrain the resolution is still not entirely adequate, nevertheless it was chosen as an operationally feasible compromise for a domain size encompassing the entire area of Austria (600 × 350 km). Another reason for using a 1 km grid is that it corresponds to the resolution of the radar data used in INCA.

In the vertical, a *z*-system is used where *z* is the height above the 'valley-floor surface'. In mountainous or hilly terrain, the valley-floors of adjacent valleys are generally found at comparable heights. Thus one may define a hypothetical surface that is smooth compared to the actual topography and connects major valley-floors (Haiden 1998). This surface represents a

useful local reference height for the *z*-System. The vertical resolution of INCA is currently equidistant at $\Delta z = 200$ m. The system has 21 levels (surface included) parallel to the valley-floor surface, covering the lowest 4000 m above this surface. For the wind analysis a *z*-coordinate with horizontal levels and $\Delta z = 125$ m is used. The irregular shape and reduced volume of grid elements intersecting the terrain is taken into account using the shaved element approach (Steppeler et al. 2002).

ALADIN forecast fields are used as a first guess for the three-dimensional INCA analyses (temperature, humidity, wind). The NWP fields are 1-hourly, at a horizontal resolution of 9.6 km, with 45 levels in the vertical. Two ALADIN forecast runs per day are performed (00Z, 12Z). Post-processed fields from these runs are available at about 05Z and 17Z. ALADIN forecast fields used in INCA are geopotential, temperature, relative humidity, u-, v-, w- wind components (3-d fields), 2m temperature and relative humidity, u-, v- 10m-wind components, precipitation, total cloudiness, and low cloudiness (2-d fields).

The most important observational dataset for the INCA system are surface stations. ZAMG operates a network of ~140 automated stations (TAWES) across the country. In the vertical, they span most of the topographic range in Austria, with highest stations Brunnenkogel (3440 m), and Sonnblick (3105 m). Although the distribution of stations is biased towards valley locations, there is a sufficient number of mountain stations to construct three-dimensional correction fields to the NWP model output on the basis of these observations. Radar data used in INCA is a 2-d composite of four radar stations with ground clutter already removed. The data has 14 intensity categories and a time resolution of 5 minutes. Due to the mountainous character of the country, radar data is of limited use in many areas in western Austria, especially during wintertime when precipitation can originate from shallow cloud systems. The Meteosat 2nd Generation (MSG) satellite provides a number of new fields as well as a higher resolution than previous Meteosat imagery. The satellite product used in INCA is 'Cloud Type' which differentiates between different cloud levels (low, medium, high) and different degrees of opaqueness.

The main conceptual difference between INCA and the Austrian analysis system VERA (Steinacker et al. 1997) is that INCA uses NWP model information for interpolation between observations, whereas VERA uses climatological information through a fingerprint method. VERA is generally run on a coarser grid and employs a more sophisticated interpolation technique. VERA generates analyses, while INCA has been designed for both analysis and nowcasting applications.

3 Convective nowcast algorithm

The INCA reference precipitation nowcast is an observation-based extrapolation which uses motion vectors determined from consecutive analyses with a correlation technique. The size of the correlation quadrangle is 100 km. Spurious correlations implying unrealistically large translation speeds are meteorologically filtered by comparison with ALADIN wind fields at 500 und 700 hPa. The filtering is done using the condition

$$\left|\vec{V}_{KORR}\right| + \left|\vec{V}_{KORR} - \vec{V}_{ALA}\right| \leq \left|\vec{V}_{ALA}\right| + 2\Delta\,, \tag{4}$$

where $\vec{V}_{KORR}$ is the motion vector derived by correlation analysis, $\vec{V}_{ALA}$ is the ALADIN 500 or 700 hPa wind (whichever is closer to $\vec{V}_{KORR}$), and Δ is a prescribed wind speed scale which determines the amount of deviation permitted between $\vec{V}_{KORR}$ and $\vec{V}_{ALA}$. Operationally, the value $\Delta = 5\,\mathrm{ms}^{-1}$ is used. Eq. (4) defines an elliptic area aligned with the vector $\vec{V}_{ALA}$. Verification of both point and areal precipitation forecasts shows that the INCA reference nowcast is superior to NWP forecasts over the first 2-4 hours.

In order to improve the convective precipitation forecast over that of a simple translation, the evolution (initiation, intensification, weakening) of convective cells must be addressed. INCA routinely generates the following convective analysis fields once every hour:

Lifted condensation level (LCL)
Level of free convection (LFC)
Convective available potential energy (CAPE)
Convective Inhibition (CIN)
Showalter index (SWI)
Lifted index (LI)
Trigger temperature deficit (DTRIG)
Equivalent potential temperature (THETA_E)
Boundary-layer flow convergence (CON)
Boundary-layer humidity convergence (MOCON)

During the period of algorithm development several different combinations of the above fields were tested. The ones which proved most useful and were ultimately used are indicated by bold letters.

The basic concept of the INCA convective nowcast algorithm is to classify each gridpoint as either 'convective' (using the condition that CAPE > 50 J kg^{-1} within a certain distance from the gridpoint) or 'non-convective'. For each convective gridpoint it is tested whether the conditions for cell initiation, cell intensification, or cell weakening are fulfilled (Table 2). In addition to the above fields, Table 2 contains criteria based on MSG satellite data, namely visible brightness and cloud type information. The visible brightness VIS is used to identify areas where non-precipitating cumulus convection is already present. It is scaled to its domain maximum value at a given time to allow use of a constant threshold value throughout the daytime diurnal cycle. It should be mentioned that the current algorithm is unable to predict initiation after sunset. Regarding MSG Cloud Type (CT) it was planned to allow initiation and intensification only in areas of convective cloud types. However, the distinction between convective and stratiform cloudiness has not yet been implemented in the CT product. Therefore, the information is only used to exclude those areas from initiation and intensification that have one of the following types: *cloud free land snow* (CT=3), *cloud free sea snow/ice* (CT=4), *high semi-transparent thin clouds* (CT=15), *high semi-transparent thick clouds* (CT=16). An additional condition, that the precipitation rate RR must be greater than a certain threshold value, had to be applied in order to avoid intensification of very small precipitation rates that are sometimes generated in the analysis as a result of station interpolation.

At each time-step the algorithm moves the precipitation field according to the motion vectors, tests whether the criteria for intensity changes are fulfilled, and performs them. The

modified precipitation field is then moved further, and so forth. All three types of intensity changes (initiation, intensification, and weakening) are modelled as a Gaussian variation in time

$$I(t) = I_{MAX} \exp\left\{ -\left[\underbrace{(t - t_{MAX})}_{t_{REL}} / \tau \right]^2 \right\}, \tag{5}$$

where the three parameters I_{MAX} (maximum rainfall rate), t_{MAX} (time of maximum rainfall rate) or rather t_{REL} (time of maximum rainfall rate relative to time t), and τ (cell evolution time-scale) are determined as follows.

In the case of initiation and intensification the cell evolution time-scale is set to the constant value $\tau_G = 30$ min. The time of maximum intensity of a newly initiated cell relative to time t is set to $t_{REL} = -2\,\tau_G$. Maximum cell intensity is parameterized as a function of specific humidity (at valley-floor level) and CAPE in the form

$$I_{MAX} = c_1 \rho q \sqrt{CAPE}\,, \tag{6}$$

where ρ=1 kg m^{-3}, and the nondimensional coefficient c_1=10. The resulting precipitation intensity at time $t + \Delta t$ is given by

$$I(t + \Delta t) = I_{MAX} \exp\left\{ -\left[(\Delta t + t_{REL}) / \tau_G \right]^2 \right\}. \tag{7}$$

For cell intensification the time relative to the time of maximum intensity is derived from the ratio of maximum intensity to intensity at time t by inverting (7) and setting $\Delta t = 0$, which gives

$$t_{REL} = -\tau_G \sqrt{\ln\left[I_{MAX} / I(t) \right]}\,, \tag{8}$$

where I_{MAX} is parameterized using (6). Precipitation intensity at time $t + \Delta t$ is again computed using (7). In the case of cell weakening it is assumed that $t_{REL} = 0$, $I_{MAX} = I(t)$. The timescale of weakening (in units of seconds) is parameterized based on moisture divergence

$$\tau_D = -\frac{c_2}{MOCON}, \tag{9}$$

where c_2=9×10^{-4}. In addition, τ_D is limited by the constraint $30 \le \tau_D \le 60$ min. Precipitation intensity at time $t + \Delta t$ is again computed using (7).

4 Results and discussion

Verification of the convective nowcast algorithm is performed for five small river catchments in different parts of the province of Lower Austria with terrain ranging from hilly (Kamp, Pulkau)

to moderately alpine (Traisen, Triesting, Piesting). Catchment sizes range from 250 km² (Piesting) to 1500 km² (Kamp). It was decided to verify areal rather than point forecasts because of their greater relevance to hydrological applications and because we did not want to penalize small location errors of the order of a few km. The forecast range considered is +15 to +120 minutes, verification measures are root mean square error (RMSE) and bias (ME) of accumulated precipitation, computed against INCA analyses. Results of the convective nowcast algorithm are compared to those obtained by pure translation. The verification period consists of all forecasts made at full hours between 11 and 18 UTC for the following days of the year 2005: May 3, 22, 23, 30, June 7, 13, 25, 27, 28, and July 25 (80 forecasts). The selected days were the ones with the highest convective rainfall amounts in Lower Austria in 2005.

When interpreting the verification results of the convective nowcast it must be kept in mind that a systematic improvement above pure translation is generally hard to achieve. By predicting intensity changes, in particular in the case of initiation and intensification, the convective nowcast takes a greater 'risk' than the translation. Our attempt was to design an algorithm that gives significant improvements in individual cases without worsening the overall skill. On the other hand, the verification periods considered here cannot be considered entirely independent since they contain cases that have been used in the design of the algorithm. Thus we expected to see improvements at least in some of the areas.

Figure 3 shows the RMSE and ME for the reference and the convective nowcast. In the non-alpine areas the results are essentially neutral. Analysis of individual cases in these areas shows a number of days where there is in fact an improvement due to the convective nowcast but this is compensated by worsening on other days. Results for the alpine areas show a significant improvement in terms of RMSE for Piesting and Traisen, and rather neutral behaviour for Triesting. In the former two areas there are also individual cases where the nowcast algorithm has a larger error than the reference, but overall the improvements dominate. One reason why the improvement is more pronounced in the alpine areas may be that, due to orographic effects, the moisture convergence is more predictable and thus better represented in the ALADIN wind field that is used as a first guess in the INCA wind analysis. The ME tends to increase slightly in areas where the RMSE is reduced. However, this is not always the case, as shown by the results for the Traisen catchment. The behaviour of the ME in relation to the RMSE shows if the improvement in RMSE is primarily due to initiation and intensification, or weakening of cells. In the Traisen catchment, the correct prediction of cell weakening dominates, whereas in the Piesting and Triesting catchments the improvement is more strongly due to initiation and intensification. These two areas also contain well-known climatological 'hot spots' for orographically triggered convective developments. With regard to differences in error magnitude between catchments it is important to note that they do not indicate a difference in forecast skill but primarily reflect different precipitation amounts.

In order to confirm whether the verification results from 2005 can be generalized, an additional continuous verification was performed which covers all nowcasts made between 4 April 2006 and 16 May 2006 during a pre-operational test run of the system. In this case no individual days were selected, thus the sample contains a mixture of non-convective and convective cases. Again, no significant change in RMSE was found for the non-alpine areas, whereas improvements similar in extent to the 2005 verification were found for two alpine areas (Triesting, Piesting) with the third (Traisen) giving neutral results.

Based on a number of individual cases, Wilson et al. (2004) provide a qualitative verification of the convective nowcast algorithm in the ANC system for up to +60 min. They

demonstrate that it outperforms the purely translational forecast in most cases but also point out that further algorithm development is needed. In contrast to INCA, the ANC obtains wind fields derived from Doppler radar as input. It is likely that such input would increase the skill of the INCA convective nowcast especially in lowland areas, where the current wind analysis based on NWP results and station data appears to be unable to resolve the convergence characteristics relevant to convective intensity changes. A quantitative evaluation, and comparison with pure translation, was made for the GANDOLF system by Pierce et al. (2000). In contrast to INCA, GANDOLF uses an object-oriented algorithm to extrapolate cell movement and intensity. For all non-frontal convective events of 1995-1996, results similar to the ones presented here were obtained in the sense that both improvements and worsening compared to pure translation (NIMROD) was found for different catchments.

5 Conclusions

An approach to convective nowcasting is presented which is based on high-resolution analyses of some key convective diagnostics. It is found that the convective analysis fields most important for the nowcast are CAPE, CIN, moisture convergence, and trigger temperature deficit. The current version of the algorithm also requires visible satellite imagery in order to identify areas of incipient cell intensification and to avoid over-prediction of cell initiation. Verification of areal precipitation nowcasts for small catchments shows that on average the convective nowcast performs slightly better than the purely translational nowcast. The improvement is more pronounced in the alpine catchments studied, whereas it is marginal in the non-alpine areas. This difference in behaviour appears to be due to the more predictable character of the orographically induced moisture convergence field along the main alpine rim as compared to that over the lowland areas.

There are many possible ways in which the current version of the algorithm could be improved. For example, it could be argued that the thresholds set for input fields like CAPE, CIN, dTtrig and MOCON should not be constants but rather depend on the values of the other fields at the given instant and location. Also, it would be more physical in terms of an ingredient-based approach to use mass convergence instead of moisture convergence. For the mesoscale structures studied here, however, the convergence term dominates MOCON, making mass and moisture convergence fields look rather similar (Banacos and Schultz 2005).

Probably the largest improvement could be gained by improved analyses of the primary fields from which the convective diagnostics are derived. The typical length scale of CAPE, CIN, and MOCON variations in the analysis is significantly larger than the scale of individual convective cells. The dTtrig parameter, which is smaller in scale, is not yet sufficiently reliable. This leaves the visible satellite imagery as the main factor determining on the meso-γ scale where convective initiation or intensification takes place. It also means that the current nowcast algorithm is unable to predict cell initiation in clear air. Further work on INCA will address this problem through improved spatial interpolation techniques for temperature, humidity and wind.

References

Banacos, P. C., and D. M. Schultz, 2005: The use of moisture flux convergence in forecasting convective initiation: historical and opeational perspectives. *Wea. Forecasting,* **20,** 351-366.

Browning, K. A., and C. G. Collier, 1989: Nowcasting of precipitation systems. *Rev. Geophys.,* **27,** 345-370.

Crook, N. A., and J. Sun, 2004: Analysis and forecasting of the low-level wind during the Sydney 2000 Forecast Demonstration Project. *Wea. Forecasting,* **19,** 151-167.

Golding, B. W., 1998: Nimrod: A system for generating automated very short range forecasts. *Meteorol. Appl.,* **5,** 1-16.

Haiden, T., 1998: Analytical aspects of mixed-layer growth in complex terrain. Preprints, *Eighth Conference on Mountain Meteorology,* Amer. Meteor. Soc., Flagstaff, Arizona, 368-372.

Haiden, T., 2001: High-resolution forecasts of mountain cumulus. Proceedings, *22nd EWGLAM / 7th SRNWP Meeting*, Toulouse, France, 134-138.

Hand, W. H., 1996: An object-oriented technique for nowcasting heavy showers and thunderstorms. *Meteorol. Appl.,* **3,** 31-41.

Li, L., W. Schmid, and J. Joss, 1995: Nowcasting of motion and growth of precipitation with radar over a complex topography. *J. Appl. Meteor.,* **34,** 1286-1300.

Pierce, C. E., P. J. Hardaker, C. G. Collier, and C. M. Haggett, 2000: GANDOLF: a system for generating automated nowcasts of convective precipitation. *Meteorol. Appl.,* **7,** 341-360.

Pierce, C. E., E. Ebert, A. W. Seed, M. Sleigh, C. G. Collier, N. I. Fox, N. Donaldson, J. W. Wilson, R. Roberts, and C. K. Mueller, 2004: The nowcasting of precipitation during Sydney 2000: An appraisal of the QPF algorithms. *Wea. Forecasting,* **19,** 7-21.

Steinacker, R., W. Pöttschacher, M. Dorninger, 1997: Enhanced Resolution Analysis of the Atmosphere over the Alps Using the Fingerprint Technique. *Annalen der Meteorologie*, **35,** 235- 237

Steppeler, J., H.-W. Bitzer, M. Minotte, and L. Bonaventura, 2002: Nonhydrostatic atmospheric modeling using a z-coordinate representation. *Mon. Wea. Rev.,* **130,** 2143-2149.

Sun, J., and N. A. Crook, 2001: Real-time low-level wind and temperature analysis using WSR-88D data. *Wea. Forecasting,* **16,** 117-132.

Wilson, J. W., and W. E. Schreiber, 1986: Initiation of convective storms by radar-observed boundary layer convergence lines. *Mon. Wea. Rev.,* **114,** 2516-2536.

Wilson, J. W., E. E. Ebert, T. R. Saxen, R. D. Roberts, C. K. Mueller, M. Sleigh, C. E. Pierce, and A. Seed, 2004: Sydney 2000 Forecast Demonstration Project: Convective storm nowcasting. *Wea. Forecasting,* **19,** 131-150.

FIGURE AND TABLE CAPTIONS

Fig. 1. Basic structure of the INCA analysis and forecasting system. For explanation see text.

Fig. 2. INCA domain and topography. Domain size is 600 × 350 km, the horizontal resolution is 1 km. River catchments referred to in this study are Kamp (1), Pulkau (2), Traisen (3), Triesting (4), Piesting (5).

Fig. 3. Verification results for the non-alpine catchments Kamp and Pulkau, and the alpine catchments Traisen, Triesting, Piesting. Shown are root mean square error (RMSE) and bias (ME) of areal precipitation nowcasts as a function of forecast time for the convective nowcast (index cn) and the pure translational nowcast (index tn).

Table 1. Meteorological fields operationally analyzed and forecast by the INCA system. SFC = surface station observations, SAT = MSG satellite data (cloud types), RAD = precipitation radar data. Convective analysis fields are derived from the temperature, humidity, and wind analysis and therefore use surface observations only indirectly.

Table 2. Convective nowcast algorithm decision criteria and threshold values for cell initiation, intensification, and weakening.

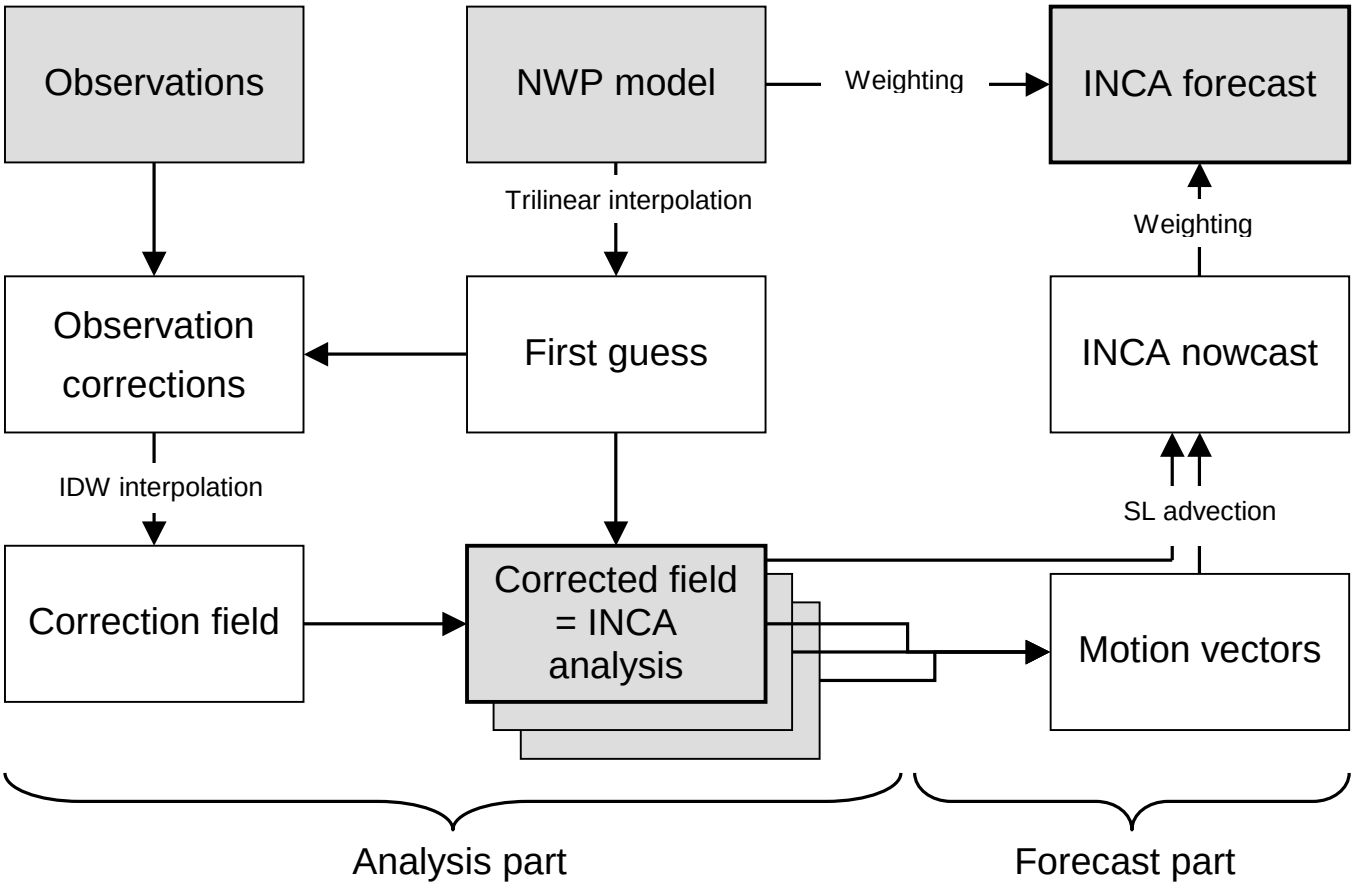
Observations
NWP model
Weighting
INCA forecast
Trilinear interpolation
Weighting
Observation corrections
First guess
INCA nowcast
IDW interpolation
SL advection
Correction field
Corrected field = INCA analysis
Motion vectors
Analysis part
Forecast part

Figure 1

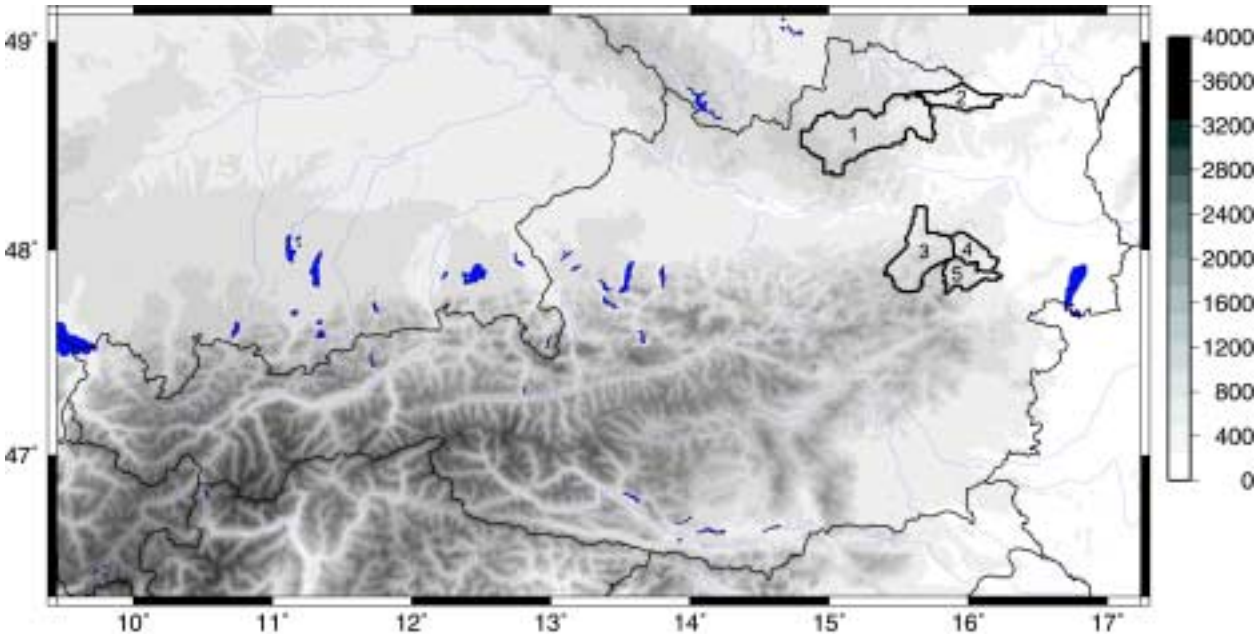
49°
48°
47°
10°
11°
12°
13°
14°
15°
16°
17°
1
2
3
4
5
4000
3600
3200
2800
2400
2000
1600
1200
800
400
0

Figure 2

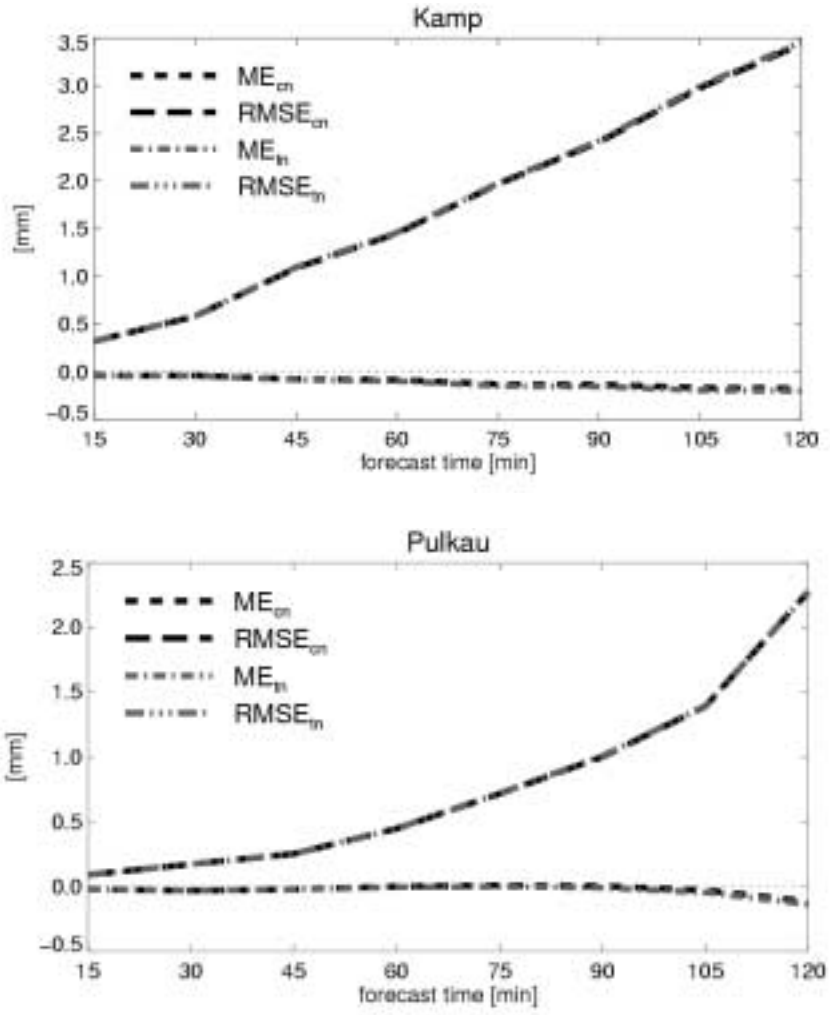

Figure 3 (continues on next page)

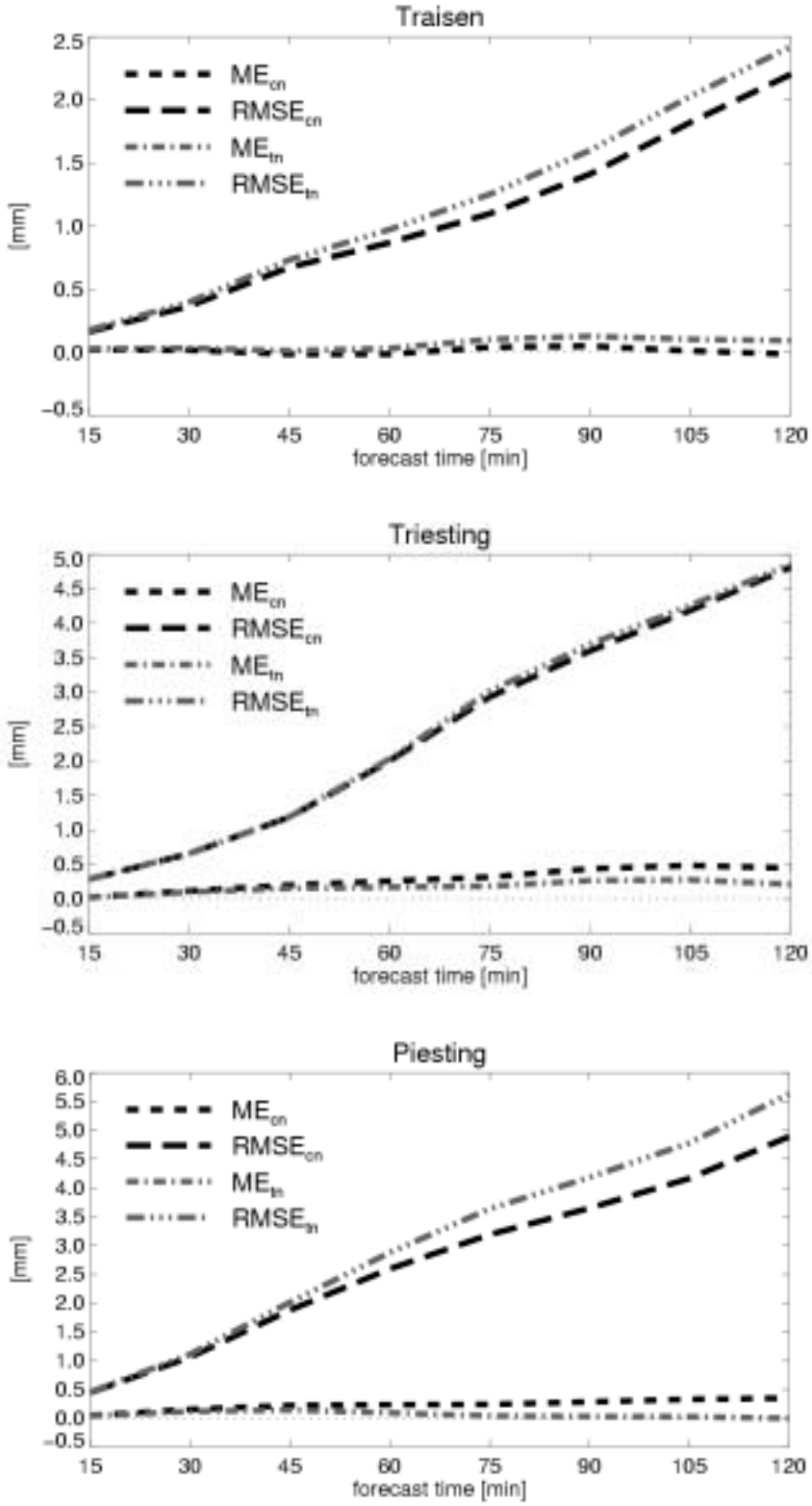

Figure 3 (continued)

Table 1

Field	Dimensionality	Update interval	Observations used	Nowcasting method
Temperature	3	1 hour	SFC	local weighting
Humidity	3	1 hour	SFC	local weighting
Wind	3	1 hour	SFC	local weighting
Cloudiness	2	15 min	SFC, SAT	motion vectors
Precipitation	2	15 min	SFC, RAD	motion vectors
Global radiation	2	1 hour	SFC, SAT	local weighting + motion vectors
Convective analysis fields	2	1 hour	(SFC)	-

Table 2

Criterion	Threshold value
Cell initiation	
CAPE > CAPEini	CAPEini = 100 J kg^{-1}
MOCON > MOCONini	MOCONini = 2×10^{-6} s^{-1}
VIS > VISini	VISini = 0.5
CT ≠ CTexcl	CTexcl = [3, 4, 15, 16]
CIN < CINini	CINini = 200 J kg^{-1}
DTRIG > DTRIGini	DTRIGini = -2 °C
Cell intensification	
CAPE > CAPEint	CAPEint = 50 J kg^{-1}
MOCON > MOCONint	MOCONint = 2×10^{-6} s^{-1}
CT ≠ CTexcl	CTexcl = [3, 4, 15, 16]
CIN < CINint	CINint = 200 J kg^{-1}
DTRIG > DTRIGint	DTRIGint = -2 °C
RR > RRint	RRint = 0.2 mm h^{-1}
Cell weakening	
RR > RRweak	RRweak = 0.0 mm h^{-1}
MOCON < MOCONweak	MOCONweak = 0.0 s^{-1}
CAPE < CAPEweak	CAPEweak = min($\overline{CAPE}^{>0}$,100 J kg^{-1})